Atmos. Meas. Tech. Discuss., 8, 3245–3282, 2015
www.atmos-meas-tech-discuss.net/8/3245/2015/
doi:10.5194/amtd-8-3245-2015

Atmospheric Measurement Techniques Discussions

Measurement of atomic oxygen in the middle atmosphere using solid electrolyte sensors and catalytic probes

M. Eberhart[1], S. Löhle[1], A. Steinbeck[2], T. Binder[1], and S. Fasoulas[1]

[1]Institute of Space Systems, University of Stuttgart, Stuttgart, Germany
[2]Airbus DS GmbH, Lampoldshausen, Germany

Received: 26 January 2015 – Accepted: 4 February 2015 – Published: 24 March 2015

Correspondence to: M. Eberhart (eberhart@irs.uni-stuttgart.de)

Published by Copernicus Publications on behalf of the European Geosciences Union.

Abstract

The atmospheric energy budget is largely dominated by reactions involving atomic oxygen (O). Modeling of these processes requires detailed knowledge about the distribution of this oxygen species. Understanding the mutual contributions of atomic oxygen and wave motions to the atmospheric heating is the main goal of the rocket campaign WADIS. It includes, amongst others, two of our instruments for the measurement of atomic oxygen that have both been developed with the aim of resolving density variations on small vertical scales along the trajectory. In this paper the instrument based on catalytic effects (PHLUX) is introduced briefly. The experiment employing solid electrolyte sensors (FIPEX) is presented in detail. These sensors were laboratory calibrated using a microwave plasma as a source for atomic oxygen in combination with mass spectrometer reference measurements. The spectrometer was in turn calibrated for O with a method based on methane. In order to get insight into the horizontal variability the rocket payload had instrument decks at both ends. Each housed several sensor heads measuring during both the up- and downleg of the trajectory. The WADIS campaign comprises two rocket flights during different geophysical conditions. Results from WADIS-1 are presented which was successfully launched in June 2013 from Andøya Rocket Range, Norway. FIPEX data was sampled with 100 Hz and yield atomic oxygen density profiles with a vertical resolution better than 10 m. Numerical simulations of the flow field around the rocket were done at several points of the trajectory to assess the influence of aerodynamic effects on the measurement results. Density profiles peak at 3×10^{10} cm^{-3} at altitudes of 93.6 and 96 km for up- and downleg respectively.

1 Introduction

Atomic oxygen (O) is a highly reactive species and a key element in a number of atmospheric processes. At high altitudes it is one of the major constituents of Earth's

AMTD
8, 3245–3282, 2015

atmosphere and may cause erosion to exposed parts of spacecraft, especially on solar panels of satellites and the space station (Reddy, 1995). In the mesosphere and lower thermosphere (MLT) O is an important carrier of chemical energy and plays a significant role in the distribution of solar energy (Hedin et al., 2009). Atomic oxygen is produced by photodissociation of O_2 and is then dispersed via various processes such as global circulation and wave motions. The chemical energy stored is released upon recombination and as the lifetime of the radicals is long in the upper regions the heating may occur at a large distance from the source, horizontally as well as vertically. On the other hand, atomic oxygen is also involved in the most important heat sink in the MLT, the radiation of CO_2 in the 15 µm-band, where the population of the relevant energy levels depends mainly on collisions with O (Mlynczak, 1996). Determination of local atomic oxygen densities is therefore a necessity for detailed modeling of the atmospheric energy budget and understanding of the underlying physical processes. The demand for high spatial resolution requires in-situ measurement techniques and the altitudes of interest leave sounding rockets as the only appropriate instrument carriers.

In order to quantify both the contribution of dissipating gravity waves and of atomic oxygen to the atmospheric heating the campaign WADIS has been set up (Gritzner and Rapp, 2011; Gritzner and Strelnikov, 2013). The project is led by the Leibniz-Institute of Atmospheric Physics (IAP) under a grant by the German Aerospace Center (DLR). Several institutions provided rocket-borne experiments for the direct measurement of small scaled turbulences and various neutral and charged particles in combination with ground based observations using radar and lidar. The campaign foresees two launches of sounding rockets in very different geophysical conditions, during winter- and summertime. The Institute of Space Systems (IRS) operates two sensor systems both designed for the determination of atomic oxygen density profiles along the trajectory.

The first instrument called FIPEX (Flux-ϕ(Phi)-Probe-Experiment) is based on solid electrolyte sensors, a technique that has been successfully flown on a number of rocket missions. On TEXUS 34 (1996) a modified commercial lambda probe was employed (Schrempp, 1996), followed by miniaturized sensors on the Russian capsules

AMTD
8, 3245–3282, 2015

IRDT (2000) and IRDT-2 (Fasoulas et al., 2001). These sensors, however, could not distinguish between molecular and atomic oxygen. A refined version with improved selectivity towards O was used in an experiment on the International Space Station (2008) (Schmiel, 2009). WADIS is the first campaign to employ this measurement principle for the determination of atomic oxygen densities aboard a sounding rocket. The sensors are very small in size, lightweight, with low power consumption and feature a high temporal and therefore spatial resolution.

The second sensor system named PHLUX (Pyrometric Heat Flux Experiment) measures temperature on two surfaces with different catalytic activities towards the recombination of atomic oxygen. The surface that promotes recombination receives a higher amount of chemical heat, leading to a temperature difference between the surfaces proportional to the incident atomic oxygen flux. Such catalytic probes have previously been used for atmospheric research on sounding rockets, albeit with a different design (Perov and Rakhmanov, 1977). We adopted a concept originally developed for ESA's re-entry capsule EXPERT (Herdrich et al., 2005).

The first sounding rocket of the WADIS campaign was launched on 27 June 2013 at Andøya rocket range in Andenes, Norway, at 23:52 UTC. The payload had two instrument decks, one fore and one aft. They were symmetrically equipped with FIPEX and PHLUX sensors, together with several other experiments: CONE (neutral and electron density, neutral temperature and turbulence, IAP), particle detector (IAP), positive ion probe (TU Graz), photometers (atomic oxygen and noctilucent clouds, MISU), Faraday antenna (absolute electron density, TU Graz), Langmuir probe (electron and charged aerosol density, Embry-Riddle). The payload had a constant, almost vertical orientation during the experimentation phase and the instrumentation of the rocket on both ends had the benefit of measurements during both up- and downleg of the trajectory which enables conclusions about the horizontal distribution of relevant parameters. An apogee of 115 km was reached, 20 km short of the planned trajectory.

In this paper we present the applied measuring principles and results from the two IRS sensor systems, with an emphasis on FIPEX data. Details about the PHLUX oper-

AMTD
8, 3245–3282, 2015

ation will be published in a companion paper. Atomic oxygen density profiles calculated from the flight data will be discussed and compared to literature.

2 Solid electrolyte sensor FIPEX

The so-called lambda-probe presents the most prominent example of a solid electrolyte oxygen sensor. It measures the oxygen concentration in automobile exhaust gases in order to regulate the motor's air-fuel ratio. This sensor type is based on a ceramic solid electrolyte, often yttria stabilized zirconia (YSZ). Due to the structure of its crystal lattice it is a conductor for oxygen anions, O^{2-}. If a suitable interface is provided gas phase oxygen may be built into this lattice. This is accomplished by applying an electronically conductive platinum electrode onto the electrolyte surface. Here a multi-step reaction occurs (e.g., Hertz, 2006, p. 24): gaseous O_2 is transported to the electrodes by bulk diffusion; it is adsorbed dissociatively on the surface; the O atoms are then driven to electrochemically active sites by surface diffusion; here oxygen is reduced in a charge transfer step to O^{2-} by electrons delivered by the electrode; the ions are built into vacant lattice sites of the electrolyte structure.

The active sites are essentially found on the so-called triple phase boundary where electrode, electrolyte and gas phase are in direct contact. As electrons are moved in the charge transfer reaction the electrical potential of the electrode changes until an equilibrium is reached. The steady state potential depends on the gas phase oxygen concentration. The potential difference $\Delta\Phi$ between two electrodes facing unequal gas compositions is given by the Nernst equation (e.g., Oldham and Myland, 1994):

$$\Delta\Phi = \frac{RT}{nF} \ln \frac{c_1}{c_2} \tag{1}$$

R is the universal gas constant, T the absolute temperature, F is Faraday's constant and n the number of electrons involved in the reaction. The oxygen concentrations

AMTD
8, 3245–3282, 2015

above two electrodes in different environments are given by c_1 and c_2. If one electrode is exposed to a defined reference atmosphere then the oxygen concentration on the other side can be determined by measuring the steady state value of $\Delta\Phi$. Such a sensor works according to the so-called potentiometric principle.

If an external voltage U_S is applied to the electrodes, superposing the Nernst potential, the system is forced out of equilibrium and oxygen ions are driven through the electrolyte from cathode to anode. This results in a net flow that is associated with an electrical current I_S measurable at the electrodes. So-called amperometric sensors make use of this principle and show a wide measurement range over several orders of magnitude of oxygen partial pressure. The net flow of oxygen ions persists if both electrodes are brought to the same environment. Without the requirement of a reference atmosphere these sensors can be designed with a compact planar layout. Commonly a third electrode is employed as a reference and the voltage U_S regulated such that the potential difference between cathode and reference is a constant value. The benefit of this is a linear dependence of the measured sensor current on oxygen pressure over a wide range.

An important factor for the sensor behavior is the electrode material. Besides being a good electronic conductor and being both thermally and chemically stable, it has to promote the dissociative adsorption of molecular oxygen. As stated before, platinum exhibits all these features (Schwandt and Weppner, 1997).

On the contrary, O_2 is not adsorbed on gold surfaces under high vacuum conditions, except in the case of impurities (Légaré et al., 1980; Pireaux et al., 1984), so that a sensor with gold electrodes responds to molecular oxygen to a much lesser degree. However, gas phase atomic oxygen is adsorbed directly here and may readily be incorporated into the described reaction chain. This provides the possibility of designing sensors with a selective response to atomic oxygen by using gold cathodes.

All the reaction mechanisms on the electrodes and in the electrolyte are temperature dependent. In particular the ion conductivity of YSZ rises exponentially with temperature (Park and Blumenthal, 1989) and requires the sensor to be heated to about

AMTD
8, 3245–3282, 2015

500 °C. It should be noted that the sensor currents for both molecular and atomic types are proportional to the flux of particles onto their surfaces and therefore respond to the total pressure if exposed to a moving medium.

The design of the amperometric sensor elements used in this paper is shown in Fig. 1. A functional YSZ film was screen printed from a paste (Tosoh Corporation, Japan) onto an alumina substrate. Two electrodes with an interdigitated layout and a third reference electrode were screen printed on top of the YSZ layer. A resistance heater was applied to the back side of the alumina plate, again by means of screen printing. Platinum paste (Ferro 64120410, Germany) was used for both the electrodes and the heater; for the electrodes the paste was mixed with YSZ-powder (Tosoh Corporation, Japan) giving a porous layer with an increased triple phase boundary. Electrodes and heater were contacted with gap welded Pt-Ni leads.

In order to obtain sensors selectively sensitive to atomic oxygen the cathode was subsequently electroplated with gold. This was achieved by placing the sensors in an electrolyte solution (no. 530522, Dr. Ropertz GmbH, Germany), with a voltage of 3.0 V applied between cathode and a stainless steel counter electrode for 3 min at a current of 10 mA.

The electrical circuit used to control and read out the sensors is shown in Fig. 2. A PI controller stabilizes the potential between cathode and reference to 300 mV by adjusting the U_S voltage. The sensor signal is the current I_S measured between anode and cathode. The sensor element is kept at a constant temperature throughout the flight by regulating the resistance heater to a defined ohmic value. Two sensors are mounted together in a common aluminum housing, one with a golden and one with a platinum cathode, as as shown in Fig. 3. The platinum sensor is sensitive to both molecular and atomic oxygen while the gold sensor selectively measures the O density. Two heat resistant ceramic elements hold the sensors in place and the leads are soldered to a LEMO connector.

This ensemble with two different sensors makes up a sensor head; to ensure redundancy three of these heads were mounted on each the fore and aft deck of the

AMTD
8, 3245–3282, 2015

payload. The sensors were operated by custom designed electronics, one on each deck, connected to the heads by a thoroughly shielded cable. The sampling frequency of the sensor data was 100 Hz. Considering the rocket speed along the trajectory this results in a theoretical vertical resolution better than 9 m during the flight. The photograph given in Fig. 4 shows the final assembly of the instruments on the fore deck of the rocket, with both a FIPEX and PHLUX sensor head visible. Pairs of heads were distributed with a 120° spacing on an adapter ring. The FIPEX sensors were mounted parallel to the rocket axis so that their sensitive electrode surface is oriented perpendicular to the main component of the flight velocity. This orientation was chosen to minimize the influence of the rocket speed onto the measured oxygen flux.

3 Catalytic probe PHLUX

Two oxygen atoms recombining on a surface release an energy of 5.2 eV (Hammer et al., 1999) leading to a temperature increase. The number of recombinations in a time interval depends on the flux of atoms onto the surface and on its catalytic activity towards this reaction, expressed by a recombination coefficient γ. The surface temperature can be related to the incident chemical heat and thus to the atomic oxygen density. To account for varying and unknown heat transfer coefficients from the surface to the surroundings a second inert probe is used. Its temperature variations reflect all other heat transfer mechanisms, like convection and radiation. In the PHLUX probe head two Pt100 temperature sensors (Heraeus type L220P, sensor area 2 mm × 2 mm) with different coatings, silicon dioxide (SiO_2) and platinum, have been placed close to each other. Platinum is a highly catalytic material, while SiO_2 is used as inert reference with γ close to zero. In order to minimize heat losses to the structure the Pt100 elements are embedded in an aerogel pad (Airloy from Aerogel Technologies Inc., USA) with extremely low thermal conduction. To account for heat losses through the sensor lead wires the temperature of the connector pins is measured by a thermocouple. Figure 5

AMTD
8, 3245–3282, 2015

shows the complete sensor head with a PEEK housing. Similar to FIPEX two heads are mounted on each payload deck for the sake of redundancy.

According to the original schedule WADIS-1 was planned in winter time, in dim light or during night. Sunlight became an obstacle to the PHLUX measurements as plans had to be shifted to summer conditions. Solar radiative heat exceeds the chemical contributions on both the coated and the uncoated surface. As the absorption coefficients and their dependence on wavelength and temperature are not known exactly the concept was altered to rule out this source of error. One of the sensor heads was covered with a sapphire window, so that the surfaces beneath do not receive any chemical heat and the temperatures represent the pure solar contributions. These values can be subtracted from the results of the uncovered head, leaving the effect from atomic recombination, if convection is assumed to be identical on both heads. This step was omitted on the aft deck as no direct sunlight was expected here.

Custom electronics were used to read the temperature of the thermocouples and the resistance of the Pt100 elements. Four-wire measurement eliminated uncertainties due to different cable lengths. Sensor data was sampled with a frequency of 1000 Hz.

4 Calibration

As no first-principles model can be employed for the interpretation of the sensor readings a laboratory calibration is necessary. This applies especially to solid electrolyte sensors, for both molecular and atomic oxygen, but more generally also to the catalytic probes. Here parameters like the catalytic efficiencies, absorption and emission coefficients or other thermo-physical properties of the sensor design are only known with high uncertainties. In the following the calibration method for the FIPEX sensors is detailed. The PHLUX sensors were calibrated for the incident heat flux density using the NISI method (Löhle et al., 2013, 2007).

A microwave generator (2.45 GHz, Sairem, France) is used to produce a low pressure oxygen plasma as a source for atomic oxygen, a technique widely employed in

AMTD
8, 3245–3282, 2015

various technical and scientific applications and well studied in literature (Lebedev, 2010). The pure oxygen plasma is sustained within a cylindrical quartz tube at an oxygen pressure of 1.0 mbar and an incident microwave power of up to 300 W. The tube has a length of 30 cm with an outer diameter of 50 mm and is mounted onto a vacuum chamber. The atomic oxygen generated in the discharge is expanded into the vacuum through a small orifice (⌀ 0.3 mm) along with undissociated molecular oxygen. This generates a fast beam with a distinct radial and axial distribution of the atomic oxygen density. In a first step the radial profile of the degree of dissociation in this beam is determined with a quadrupole mass spectrometer (QMS, Hiden HAL 3F with cross beam ion source). The QMS is mounted on a flexible bellow with its axis perpendicular to the beam. A mechanism allows variation of the radial position of the QMS thus recording the desired profile. The degree of dissociation is obtained as the ratio between the readings at mass numbers 16 (O) and 32 (O_2). To suppress dissociative products in the ion source, which corrupt the measurement, a low electron energy of 16 eV is used. As the QMS is operated with non standard parameters it in turn has to be calibrated. For this purpose we employ a method involving methane CH_4 that shares mass number 16 with atomic oxygen (Agarwal et al., 2004). It should be stressed that the mass spectrometer only determines static number densities regardless of the velocity of the medium (Singh et al., 2000). However, the calibration of the sensors requires knowledge of the flux of O atoms in the beam. Therefore a second measurement is required to provide the total flux which can be combined with the degree of dissociation to form the profile of atomic oxygen total pressure needed for calibration. This measurement is made in the pure O_2 beam (plasma off) with a solid electrolyte sensor with platinum electrodes calibrated for O_2 under static conditions. As the beam profile is radially symmetric this sensor is mounted on a linear/rotary manipulator (MDC BRLM-275) opposing the QMS, together with the atomic oxygen sensor to be calibrated. After the total flux profile has been determined the manipulator is turned about 180°, so that the second sensor is exposed to the beam and its response to the radially varying atomic flux (plasma on) can be recorded. This enables an almost simultaneous operation of

AMTD
8, 3245–3282, 2015

the O sensor and the QMS reference system without the need of opening the vacuum chamber between measurements.

Calibration curves for atomic oxygen obtained by this procedure are given in Fig. 6 for the sensors used during WADIS-1.

Calibration for molecular oxygen is done by testing the sensors in a vacuum chamber under stationary conditions. The partial pressure of O_2 is varied by a leak valve (Balzers UDV 235) and the sensor current measured against a pressure gauge (Pfeiffer FullRange PKR251). Results for one sensor with platinum cathodes are plotted exemplarily in Fig. 7. All sensors with gold cathodes showed almost no sensitivity towards molecular oxygen in the relevant pressure range.

5 Aerodynamic considerations

It is important to consider that the measurements conducted on sounding rockets are intrusive because the rocket itself influences the flow field of the medium to be analyzed. The high velocities produce complex patterns of shock- and rarefaction waves with regions of very different temperatures and densities than in the undisturbed atmosphere. Due to their different masses and thermal velocities the abundance of the various species may additionally be altered in the vicinity of the rocket walls (Bird, 1988). All such effects have to be taken into account when making conclusions on atmospheric properties from the measurement results. Exceptions are instruments with cryogenically cooled surfaces like the mass spectrometers flown on several missions (Offermann et al., 1981). Here incident particles are trapped on the cold walls and the shock is "frozen out" as no reflections occur. This, however, requires intensive cooling with liquid helium to temperatures below 20 K which dramatically increases the system complexity. Optical methods may operate on a boom deployed from the rocket to probe a volume well outside of the shock front (Hedin et al., 2009). Here aerodynamic simulations are required to reveal the position and extent of the disturbances to appropriately design the detection system.

AMTD
8, 3245–3282, 2015

In order to investigate the aerodynamic effects during the flight, we conducted simulations of the flow field at distinct points of the trajectory. These computations have to account for the transition of the flow regime from continuum to free molecular flow across the mesopause region, which cannot be treated by classical continuum mechanics. As indicated in Fig. 8 the WADIS payload had an almost vertical orientation throughout the whole experimentation phase so that three dimensional aerodynamics have to be considered due to the horizontal velocity component.

The Direct Simulation Monte Carlo method (DSMC) of the PICLas-code, developed in collaboration between IRS and the Institute of Aerodynamics and Gas Dynamics (IAG) (Munz, 2014), was employed to simulate the flow conditions at five points on the downleg part of the trajectory. For collisions a pairing scheme including the Natural-Sample-Size method with a nearest neighbor search and a standard (variable hard sphere, VHS) model was applied in which the energy dependent collision cross section is derived from viscosity data by $\mu \propto T^{\omega}$ ($\omega = 0.75$ used). The species Ar, O, N_2 and O_2 were considered in the calculation with a VHS reference temperature of 273 K. For the VHS reference diameters values of 4.17 Å (Ar), 3.1 Å (O), 4.17 Å (N_2) and 4.07 Å (O_2) were used.

The internal degrees of freedom of the molecules were taken into account while neglecting chemical reactions. Each particle in the simulation represented between 1.5×10^{11} and 2×10^{13} real particles (macro particle factor, MPF). The computational domain includes an unstructured, hexahedral mesh with cell edge lengths between 3 and 50 mm and rectangular boundaries with minimal distances to the body ranging from 0.5 to 1.3 m. Symmetry of the rocket was exploited by simulating only one half of the domain. The sensor heads were included in the calculation with simplified block-like geometries with the approximate size of two adjoined heads. Apart from the actual triangular configuration, see sketch in Fig. 4, two of these blocks were positioned on adjacent sides of the rocket axis in order to cover both the maximal and minimal particle density cases during one revolution of the rocket. On the walls a diffusive reflection with full accommodation and a temperature of 300 K was assumed, whereas specular

AMTD
8, 3245–3282, 2015

reflection was set for the plane of symmetry. All other boundaries were open with an inflow from a virtual buffer layer filled with particles of a Maxwell-Boltzmann distribution corresponding to the free stream condition. Steady state, i.e. start of averaging of macroscopic values, such as particle density, was assumed to be reached after 0.02 s. The gas composition at the different altitudes was taken from the standard MSIS-E-90 model, temperatures from the CONE results. Sensitivity analyses were conducted in terms of varying boundary distances and MPFs. Computing time for the simulations ranged from 0.5 to 4 h on 96 cores of a CRAY XC40 for altitudes above 85 km and was 10 h on 192 cores for the 85 km case. Flow field results for 85 and 100 km altitude are given exemplarily in Fig. 9. Here the ratio of the local total number density (n) to the value of the undisturbed atmosphere (n^{∞}) is plotted. At 85 km a distinct shock is formed with pronounced ram and wake regions that are blurred towards higher altitudes. The values of n/n^{∞} on the upwind side at the sensor position are given in Fig. 10 as a function of altitude, with one line each representing the ram and wake sensors. The n/n^{∞} values were multiplied to the measurement results to correct for aerodynamic effects. Due to computational reasons only the total number densities could be considered for this ratio; in previously published simulations, however, the relative abundance of O was shown to vary only slightly (Hedin et al., 2009).

6 Results

In the following the results from the FIPEX measurements before and after aerodynamic correction are given. Emphasis is laid on the atomic oxygen density profiles; values for molecular oxygen, obtained from the platinum cathode sensors, and PHLUX results are presented briefly.

AMTD
8, 3245–3282, 2015

6.1 FIPEX – atomic oxygen profiles

An overview of the raw signals obtained from all atomic oxygen sensors is given in Fig. 8. The values are plotted vs. the duration of the flight, together with the altitude and significant events. Additionally the orientation of the rocket payload with instrument decks on both ends is shown. Due to their alignment the sensors were affected by the horizontal component of the flight velocity. As the rocket was spin stabilized this resulted in a signal modulated with a 2.9 Hz-component that was removed with a notch filter. One sensor on the lower deck showed unstable oscillations in the signal and was excluded from further analysis, so that in total results from 5 O sensors could be used. After application of the respective calibration curves atomic oxygen partial pressures were obtained. Number densities were calculated by dividing by kT, were k is Boltzmann's constant and T the local absolute temperature measured with high spatial resolution by the CONE instrument. Temperature data was not available for altitudes above 110 km.

Fore sensors

Data obtained from the fore sensors before aerodynamic correction is given in Fig. 11. Corrected profiles are plotted in Fig. 14. In the initial phase, after nosecone separation at 53 km altitude, the sensors had to accommodate to the low density conditions of the free atmosphere and show very different results. They measured in the rocket ram during ascent and stayed in the wake during descent. The profiles are plotted from an altitude of 80 km upwards where they converge at 91 km to form a sharp rise in atomic oxygen number density. From that point onwards the curves follow each other qualitatively with a maximum deviation of 2.5×10^{10} cm^{-3} at their peak value at 93.6 km altitude. During downleg variations in the O density can still be resolved, with two profiles closely matching (C17 and B22) while the third one (C15) differs. The characteristics obtained by the first mentioned sensors are similar to the ascent results while their magnitude is reduced by a factor of about 3, with less details than during upleg.

AMTD
8, 3245–3282, 2015

Aft sensors

The motor was separated at an altitude of 60.9 km releasing the lower instrument deck. Profiles recorded by the aft sensors are plotted in Fig. 12, again without application of the aerodynamic correction factors. Corrected results are included in Fig. 14. While in the wake, during ascent, no density variations could be determined. For both sensors the downleg profile is dominated by a deep dip with a minimum between 104 and 106 km, followed by a gradual rise that peaks at 96 km altitude. Below that point a characteristic sharp gradient and small-scaled variations are observed, followed by a sharp gradient at an altitude of 87 km. The high frequency fluctuations in the lower part of the curves are probably leftovers from the rocket spin. The payload enters flat spin at around 68 km which terminates the measurements. Below 85 km the results suffer from increasing noise that may be due to a beginning instability in the flight state or due to increasing thermal load at higher density levels.

6.2 FIPEX – molecular oxygen

Results for the molecular oxygen number density recorded by sensor C24 (fore deck) during the upleg and downleg after aerodynamic correction are plotted exemplarily in Fig. 13. Here the calibration curve given in Fig. 7 was applied to the raw signal after filtering out the spin modulations. This practice neglects the fact that the platinum electrodes also respond to atomic oxygen, although with a different characteristic than to O_2 due to differing adsorption kinetics. On the one hand the binding energy of the molecule has to be supplied for the dissociative adsorption to take place and on the other hand the probability of finding suitable neighboring adsorption sites for both atoms on the surface is lower than in the case of a single incident O atom. The complete calibration of a platinum sensor for mixtures of O_2 and O is therefore more complex than in the case of gold electrodes that do not respond to molecular oxygen. For this reason the results cannot be understood as pure O_2-profiles but represent in some way the sum of atomic and molecular oxygen number densities.

AMTD
8, 3245–3282, 2015

The FIPEX profile obtained by the fore sensor C24 during the upleg is qualitatively very similar to the MSIS curve while being lower in absolute values. The altitude of 93 km is marked by the sharp rise in atomic oxygen density that begins to influence the O_2 results.

7 Discussion

The FIPEX density profiles after application of the aerodynamic corrections are given in Fig. 14. Additionally, results from the PHLUX measurements are plotted and data is compared to the standard MSIS-E-90 model. Though having been measured in different geophysical conditions profiles obtained during the NLTE-2 campaign, launched at Esrange rocket range, northern Sweden, on 6 March 1998, are additionally included for comparison (Hedin et al., 2009).

A fair agreement is observed for the altitude of maximum O number densities between the FIPEX results and the MSIS and NLTE-2 data. FIPEX profiles peak at 93.6 and 96 km for the up- and downleg, respectively. The MSIS-E-90 curve shows a peak value at 93.5 km and the NLTE-2 measurements recorded a maximum at 97.5 km altitude. The NLTE-2 results have a much higher spatial resolution (smoothed to 250 m on the vertical axis) than the MSIS profile and feature several distinct local extrema. The absolute peak values for n_0 from MSIS and NLTE-2 are higher than the FIPEX results by factors of 5 and 14, respectively.

Both fore and aft sensors recorded variations in atomic oxygen number density on a scale that is beyond the spatial resolution of the MSIS-E-90 and NLTE-2 profiles. The results show local extrema that can mostly be found in the curves recorded from the others sensors on the same instrument deck while they differ slightly in altitude and absolute value between upleg-fore and downleg-aft measurements. These differences might be interpreted as horizontal variations in O density as the trajectory spans over a distance of about 30 at 80 km altitude. The broad minimum observed in the downleg-aft profiles at around 105 km altitude, is, however, most likely not due to actual large

AMTD
8, 3245–3282, 2015

variations in the atomic oxygen concentration; the fore sensor data does not show this feature. One attempt for explaining this situation could be made by assuming the onset of outgassing on the rocket rear side beyond apogee. The surfaces would heat up due to an evolving bow shock releasing adsorbed particles, e.g. exhaust gases, that consume atomic oxygen in chemical reactions. However, the increase in surface temperature measured by the PHLUX sensors between apogee and 105 km was only about 0.5 K, so that outgassing does not seem to cause an atomic oxygen depletion. We favor an interpretation based on the electrode kinetics. As laid out before the reference voltage of the sensor is regulated to a constant value by appropriately adjusting U_S, the voltage between anode and cathode. With increasing oxygen concentration U_S has to be raised which leads to a linear characteristic of the sensor current over a wide pressure range. Under steady state conditions a given oxygen density can be attributed to a certain ratio of U_S and I_S values. During downleg a rise in this ratio along with a decline in the absolute U_S value can be found in the aft sensor data, see Fig. 15, exactly at the altitude were the dip in O density was observed. Although the gold coated cathode is not sensitive towards molecular oxygen the platinum reference electrode still dissociatively adsorbs O_2. Its reduction to O^{2-} consumes electrons which increases the potential difference between reference and cathode. Subsequently U_S is lowered by the controller to maintain a constant reference voltage, leading to a decrease in I_S. This mechanism is believed to cause the dip in the signal after the sensors left the rocket wake with a very low O_2 density beyond apogee.

At very low ambient pressures the coverage of the electrode surfaces with adsorbed oxygen is also low. For two reasons the coverage on the cathode is further reduced compared to the other electrodes: firstly, gold prevents adsorption of molecular oxygen with only very low O concentrations in the rocket wake and, secondly, adsorbed O is pumped away by the applied voltage U_S. Surface diffusion to the triple phase boundary is slowed down at these low coverages so that a steady state is reached only after long periods (Förstner, 2003, p. 106). The described slow kinetics may also explain the delayed onset of the effect some seconds beyond apogee.

AMTD
8, 3245–3282, 2015

Further investigations into the transient reaction of the sensors at very low pressures have to be carried out; this will also help to improve the interpretation of high frequency variations of the results in that regime.

For upcoming missions the use of sensors with all-golden electrodes should be considered to eliminate the issues generated by different reactions on different electrode materials. A further consequence of the findings described here might be an operation of sensors with a fixed U_S, i.e. without regulating the reference voltage. This helps to maintain the electrical conditions used during laboratory calibrations at the expense of increased nonlinearity of the calibration curve.

It should be noted that the sensor currents measured during the flight, see Fig. 8, exceed the signals given in the calibration curves, see Fig. 6. Their linear characteristics had to be extrapolated by a factor of approximately 3.5. At a certain pressure the respective curves will become nonlinear. This is a gradual transition and depends on parameters such as material, surface, geometry and temperature of the electrodes and the electrolyte. If the flux of oxygen delivered by the electrodes via surface diffusion exceeds the rate at which it can be transported to the anode the current-pressure curve flattens. For the molecular oxygen sensors this is observed at currents beyond 10 µA, see Fig. 7. The O sensors differ in a thin layer of gold on the cathode which will only very slightly alter its total surface area or the length of the three phase boundary, so that a linear behavior is assumed here up until the levels observed in the flight. Neglecting an actual nonlinearity in the characteristics, however, would lead to an underestimation of the number densities, which might contribute to the differences in absolute values between measured profiles and the MSIS-standard or the NLTE-2 results.

Generally speaking the results recorded in the ram, i.e. the fore-upleg and aft-downleg profiles, appear to reflect the actual variations better than their counterparts in the wake. In the ram the measurements are also influenced by aerodynamic effects, but the response to density variations is obviously more direct, showing fluctuations on a smaller scale with a better signal-to-noise ratio. Additionally, here not the full length of the rocket has to be considered in numerical calculations when trying to simulate the

AMTD
8, 3245–3282, 2015

flow conditions along the trajectory. Though different in magnitude it is nevertheless informative to compare the fore- and aft-results during downleg as given in Fig. 16. Here the values of the fore-sensor B22 have been scaled by a factor of 3. Below 98 km altitude most of the small scaled features of the aft deck sensor CO2 can also be found in the B22 curve at the same altitude. The fact that these results are simultaneously recorded at opposite ends of the rocket with different sensors on individual electronics increases confidence that actual atmospheric O density variations are represented.

8 Conclusions

The FIPEX instrument, based on solid electrolyte sensors, was for the first time used to measure atomic oxygen number densities on a sounding rocket and has successfully recorded profiles along the trajectory of WADIS-1. On a qualitative basis the results compare well with the MSIS standard atmosphere and the profiles obtained in the NLTE-2 campaign, but exceeding their resolution and recording O density variations on small spatial scales. By symmetrical instrumentation on fore and aft deck it was possible to measure profiles both during the up- and downleg, which enables the detection of O density variations on a horizontal scale. The absolute values measured with FIPEX are by factors of around 5 to 14 lower than the mentioned references. This might be due to nonlinearities in the sensor characteristics at higher atomic oxygen densities that could not be covered in the laboratory calibration. Here further investigations are needed. For upcoming missions sensors with all golden electrodes should be considered which may eliminate disturbances through different reactions of oxygen on platinum/gold electrodes. Profiles for O number densities could also be calculated from PHLUX data, despite difficulties caused by solar radiation. If shifted upwards by 16 km these profiles are qualitatively comparable to FIPEX results.

Acknowledgements. This work has been funded by the German Aerospace Center (DLR) under grant 50 OE 1001. We thank J. Hedin from MISU, Stockholm, for providing the NLTE data and B. Strelnikov, IAP Kühlungsborn, for the CONE temperature results. We appreciate the

AMTD
8, 3245–3282, 2015

work from M. Hartling, IRS electronics lab, who designed the sensor electronics. The efforts of DLR MORABA and the support during the launch campaign are highly recognized. The platinum electrode sensors have been produced by ESCUBE GmbH in collaboration with our institute.

References

Agarwal, S., Quax, G., van de Sanden, M. C. M., Maroudas, D., and Aydil, E.: Measurement of absolute radical densities in a plasma using modulated-beam line-of-sight threshold ionization mass spectrometry, J. Vac. Sci. Technol. A, 22, 71–81, doi:10.1116/1.1627767, 2004. 3254

Bird, G. A.: Aerodynamic effects on atmospheric composition measurements from rocket vehicles in the thermosphere, Planet. Space Sci., 36, 921–926, doi:10.1016/0032-0633(88)90099-2, 1988. 3255

Fasoulas, S., Förstner, R., and Stöckle, T.: Flight test of solid oxide micro-sensors on a Russian reentry probe, in: Space 2001 Conference and Exhibition, 28–30 August 2001, Albuquerque, USA, 2001. 3248

Förstner, R.: Entwicklung keramischer Festelektrolytsensoren zur Messung des Restsauerstoffgehalts im Weltraum, PhD thesis, Institute of Space Systems, University of Stuttgart, Germany, 2003. 3261

Gritzner, C. and Rapp, M.: ECOMA and WADIS, DLR Countdown, Bonn, available at: http://www.dlr.de/rd/Portaldata/28/Resources/dokumente/Publikationen/Countdown/C15_HiRes.pdf (last access: 3 March 2015), 2011. 3247

Gritzner, C. and Strelnikov, B.: Rough Seas in the Middle Atmosphere, DLR Countdown, Bonn, available at: http://www.dlr.de/rd/Portaldata/28/Resources/dokumente/Publikationen/Countdown/Countdown_23_hires.pdf (last access: 3 March 2015), 2013. 3247

Hammer, B., Hansen, L. B., and Norskov, J. K.: Improved adsorption energetics within density-functional theory using revised Perdew-Burke-Ernzerhof functionals, Phys. Rev. B, 59, 7413–7421, doi:10.1103/PhysRevB.59.7413, 1999. 3252

Hedin, J., Gumbel, J., Stegman, J., and Witt, G.: Use of O_2 airglow for calibrating direct atomic oxygen measurements from sounding rockets, Atmos. Meas. Tech., 2, 801–812, doi:10.5194/amt-2-801-2009, 2009. 3247, 3255, 3257, 3260

AMTD
8, 3245–3282, 2015

Herdrich, G., Auweter-Kurtz, M., Fertig, M., Löhle, S., Pidan, S., and Winter, M.: Present design of the flight instrumentations pyrex, phlux and respect for the capsule expert, in: Fifth European Symposium on Aerothermodynamics for Space Vehicles, edited by: Danesy, D., Vol. 563 of ESA Special Publication, Cologne, Germany, 401–408, 2005. 3248
Hertz, J. L.: Microfabrication Methods to Improve the Kinetics of the Yttria Stabilized Zirconia-Platinum-Oxygen Electrode, PhD thesis, Massachusetts Institute of Technology, 2006. 3249
Lebedev, Y.: Microwave discharges: generation and diagnostics, J. Phys. Conf. Ser., 257, 012016, doi:10.1088/1742-6596/257/1/012016, 2010. 3254
Légaré, P., Hilaire, L., Sotto, M., and Maire, G.: Interaction of oxygen with Au surfaces: a LEED, AES and ELS study, Surf. Sci., 91, 175–186, doi:10.1016/0039-6028(80)90078-3, 1980. 3250
Löhle, S., Battaglia, J.-L., Batsale, J.-C., Enouf, O., Dubard, J., and Filtz, R.-R.: Characterization of a heat flux sensor using short pulse laser calibration, Rev. Sci. Instrum., 78, 053501, doi:10.1063/1.2736388, 2007. 3253
Löhle, S., Fuchs, U., Digel, P., Hermann, T., and Battaglia, J.-L.: Analysing inverse heat conduction problems by the analysis of the system impulse response, Inverse Probl. Sci. En., 22, 297–308, doi:10.1080/17415977.2013.780170, 2013. 3253
Mlynczak, M. G.: Energetics of the middle atmosphere: theory and observation requirements, Adv. Space Res., 17, 117–126, doi:10.1016/0273-1177(95)00739-2, 1996. 3247
Munz, C.-D.: Coupled particle-in-cell and direct simulation Monte Carlo method for simulating reactive plasma flows, C.R. Mécanique, 342, 662–670, doi:10.1016/j.crme.2014.07.005, 2014. 3256
Offermann, D., Friedrich, V., Ross, P., and von Zahn, U.: Neutral gas composition measurements between 80 and 120 km, Planet. Space Sci., 29, 747–764, doi:10.1016/0032-0633(81)90046-5, 1981. 3255
Oldham, K. B. and Myland, J. C.: Fundamentals of Electrochemical Science, Academic Press, San Diego, 1994. 3249
Park, J. H. and Blumenthal, R. N.: Electronic transport in 8 mole percent Y2O3-ZrO2, J. Electrochem. Soc., 136, 2867–2876, doi:10.1149/1.2096302, 1989. 3250
Perov, S. P. and Rakhmanov, A. S.: Atomic oxygen concentration measurements by a rocket near the mesopause, in: Space Research XVII, Vol. 17, 261–264, 1977. 3248
Pireaux, J. J., Chtaïb, M., Delrue, J. P., Thiry, P. A., Liehr, M., and Caudano, R.: Electron spectroscopic characterization of oxygen adsorption on gold surfaces: I. Substrate impu-

AMTD
8, 3245–3282, 2015

rity effects on molecular oxygen adsorption in ultra high vacuum, Surf. Sci., 141, 211–220, doi:10.1016/0039-6028(84)90206-1, 1984. 3250
Reddy, M. R.: Effect of low earth orbit atomic oxygen on spacecraft materials, J. Mater. Sci., 30, 281–307, doi:10.1007/BF00354389, 1995. 3247
Schmiel, T.: Entwicklung, Weltraumqualifikation und erste Ergebnisse eines Sensorinstruments zur Messung von atomarem Sauerstoff im niedrigen Erdorbit, PhD thesis, Institute of Aerospace Engineering, Technische Universität Dresden, 2009. 3248
Schrempp, C.: Direct measurement of oxygen during a ballistic flight on a sounding rocket, in: 19th Advanced Measurement and Ground Testing Technology, doi:10.2514/6.1996-2231, 1996. 3247
Schwandt, C. and Weppner, W.: Kinetics of oxygen platinum-stabilized zirconia and gold-stabilized zirconia electrodes under equilibrium conditions, J. Electrochem. Soc., 144, 3728–3738, doi:10.1149/1.1838083, 1997. 3250
Singh, H., Coburn, J. W., and Graves, D. B.: Appearance potential mass spectrometry: discrimination of dissociative ionization products, J. Vac. Sci. Technol. A, 18, 299–305, doi:10.1116/1.582183, 2000. 3254

AMTD
8, 3245–3282, 2015

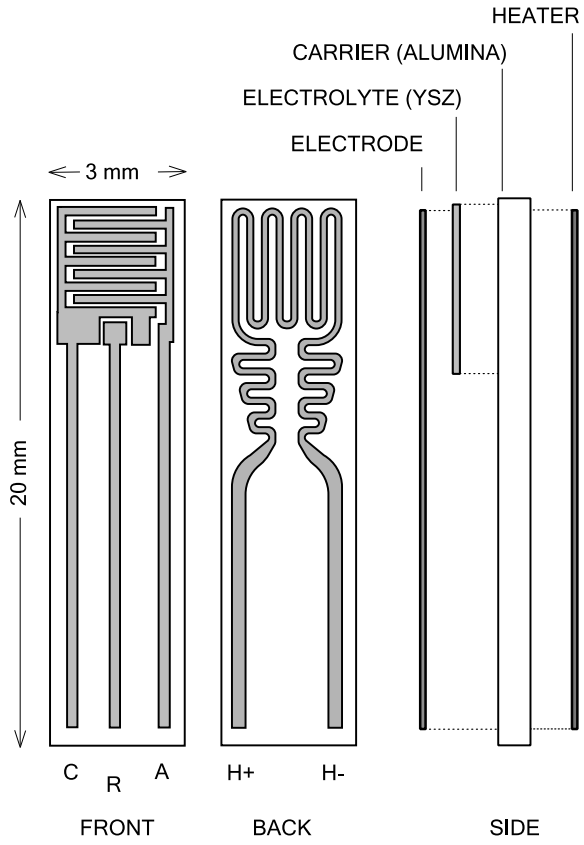

Figure 1. Layout of a FIPEX-sensor. Electrodes are made of platinum, for atomic oxygen sensors the cathode is additionally gold coated.

AMTD
8, 3245–3282, 2015

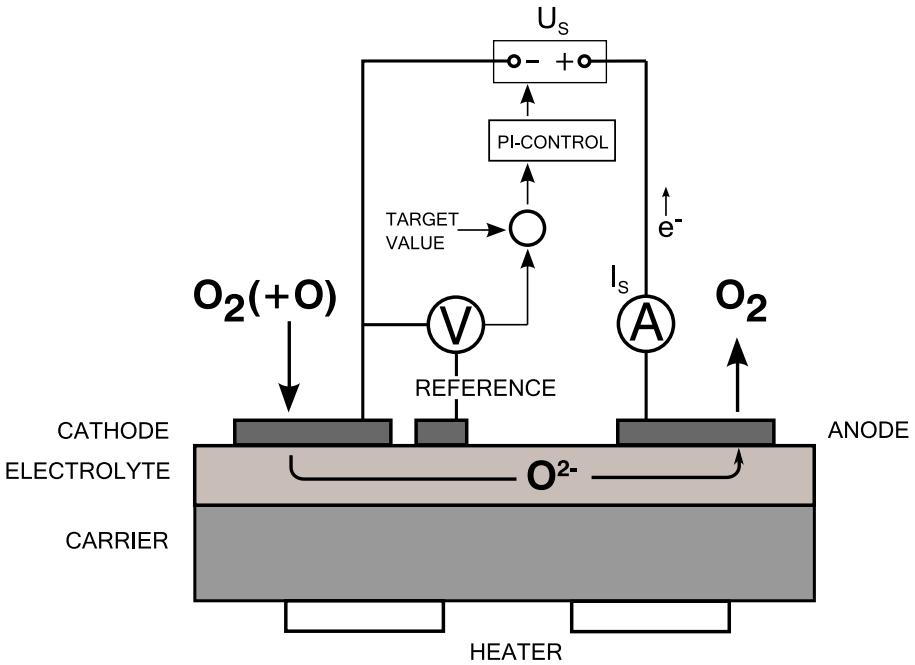

Figure 2. Electrical circuit of a sensor with 3-electrode design and regulation of the reference voltage.

AMTD
8, 3245–3282, 2015

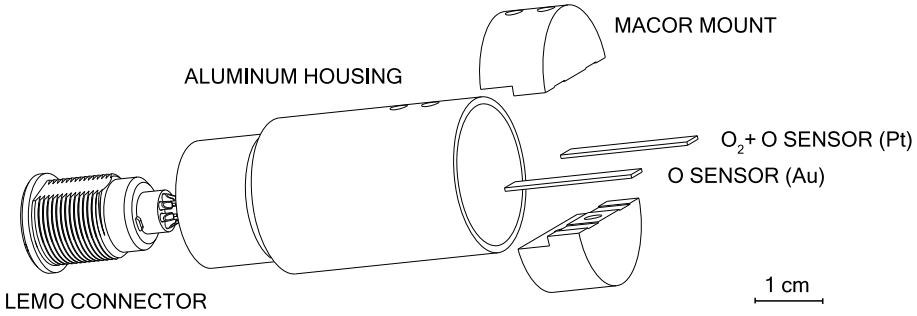

Figure 3. FIPEX head with two sensors (O and O + O_2) mounted in a common housing.

AMTD
8, 3245–3282, 2015

Figure 4. Payload on the fore deck of the rocket with both a FIPEX and PHLUX sensor head visible and a sketch showing their arrangement.

AMTD
8, 3245–3282, 2015

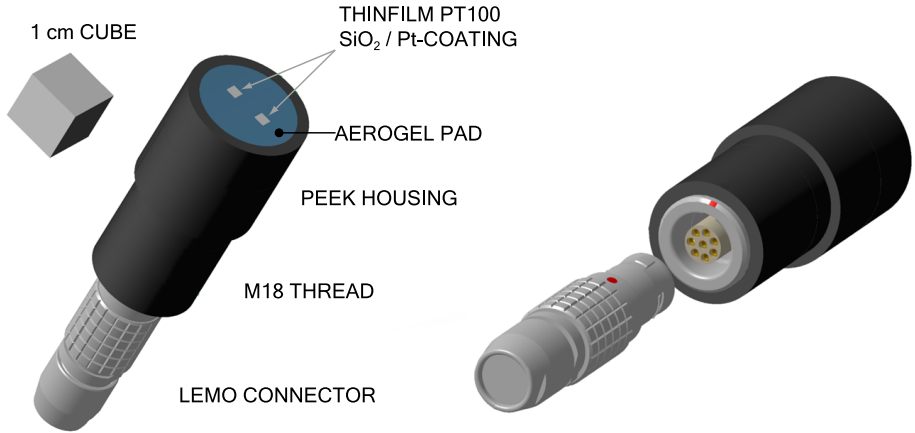

Figure 5. Design of the PHLUX sensor head.

AMTD
8, 3245–3282, 2015

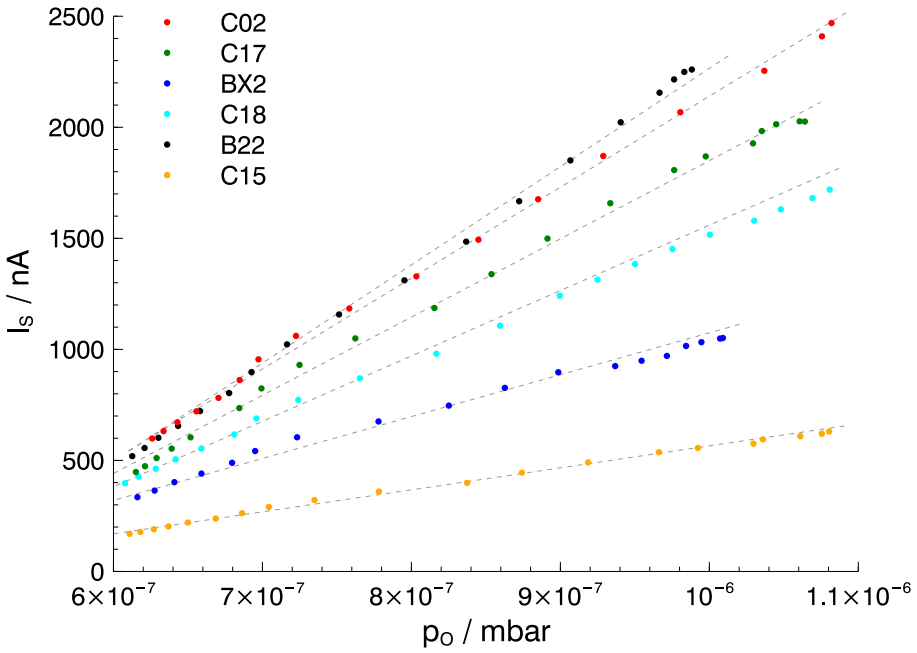

Figure 6. Calibration curves for atomic oxygen sensors on WADIS-1.

AMTD
8, 3245–3282, 2015

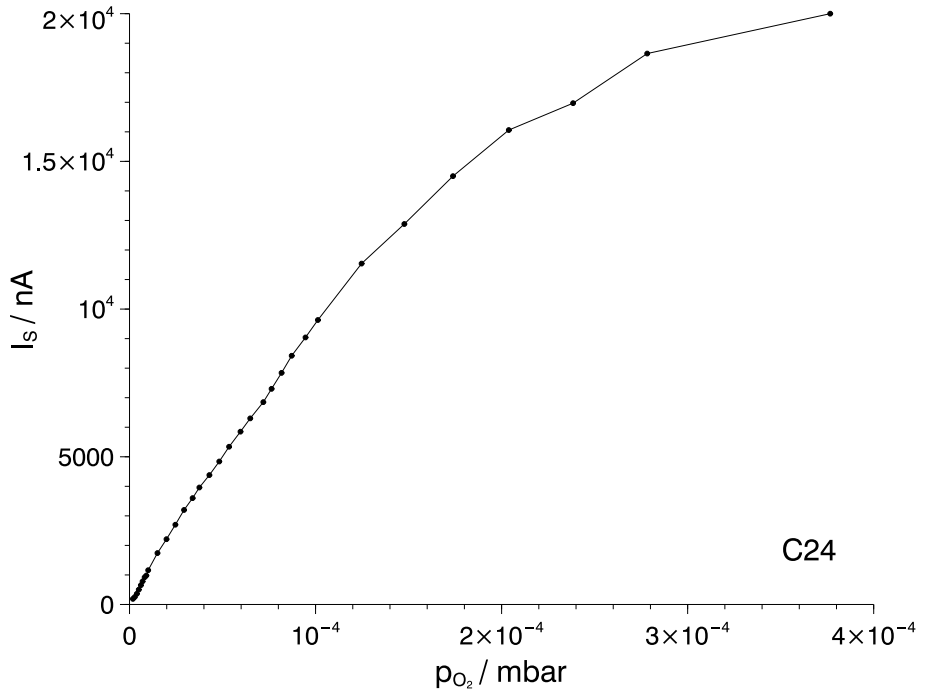

Figure 7. Calibration curve for molecular oxygen sensor C24 with platinum electrodes.

AMTD
8, 3245–3282, 2015

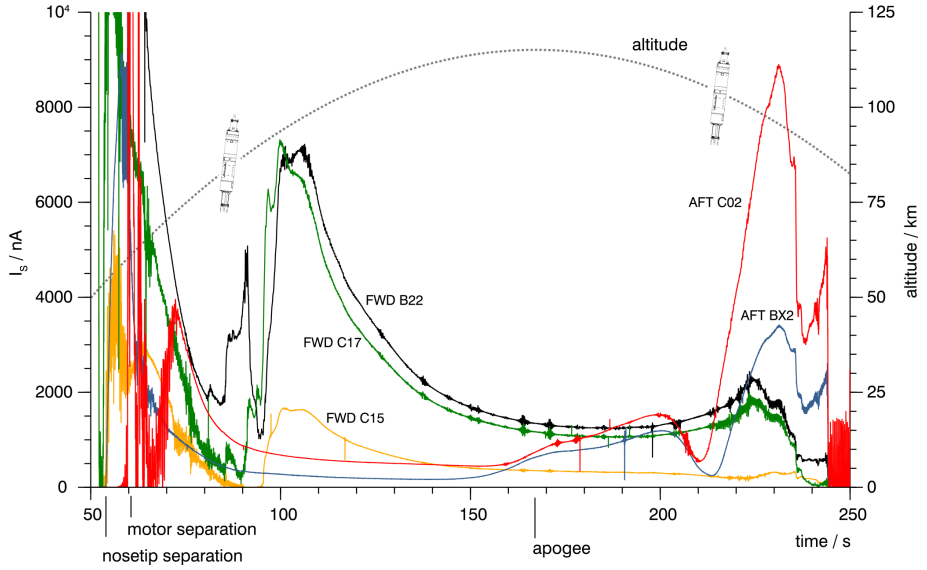

Figure 8. Raw signals of the atomic oxygen sensors vs. flight time, together with the altitude and rocket orientation during the experimentation phase.

AMTD
8, 3245–3282, 2015

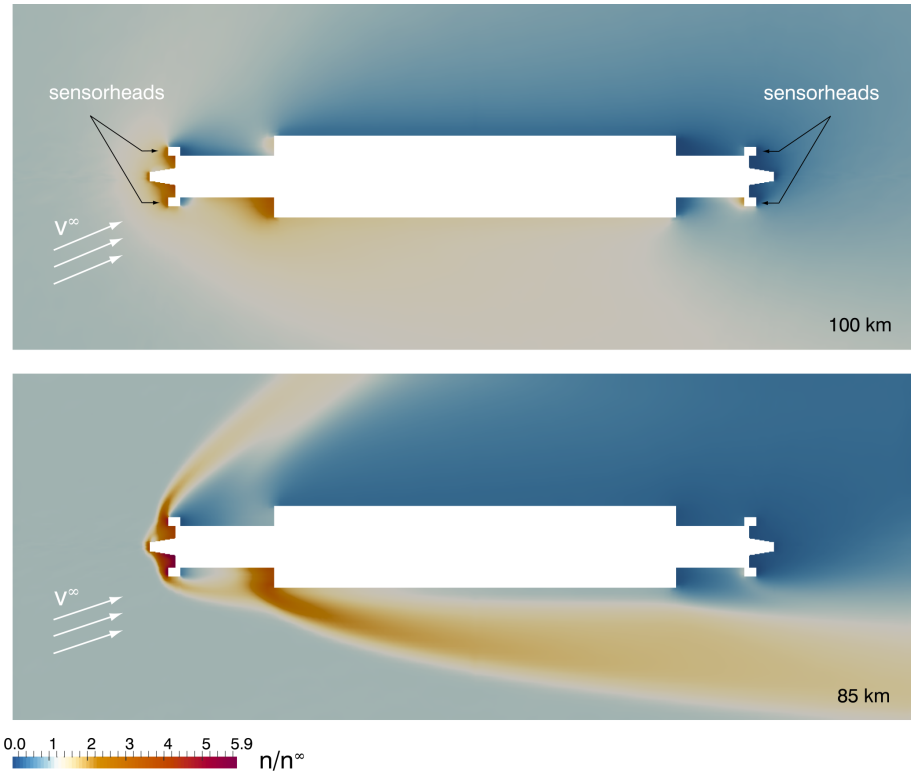

Figure 9. Distribution of the ratio between local and free stream number density during downleg at two different altitudes. Results from 3-D DSMC calculations with the PICLas-code.

AMTD
8, 3245–3282, 2015

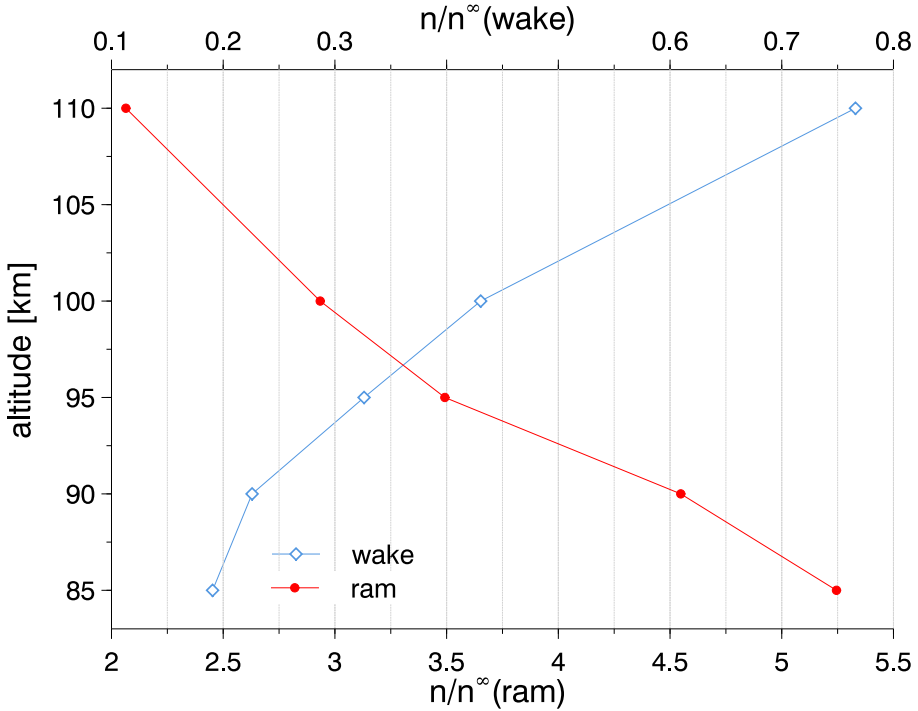

Figure 10. Ratio between local and free stream number density at the sensor position as a function of altitude.

AMTD
8, 3245–3282, 2015

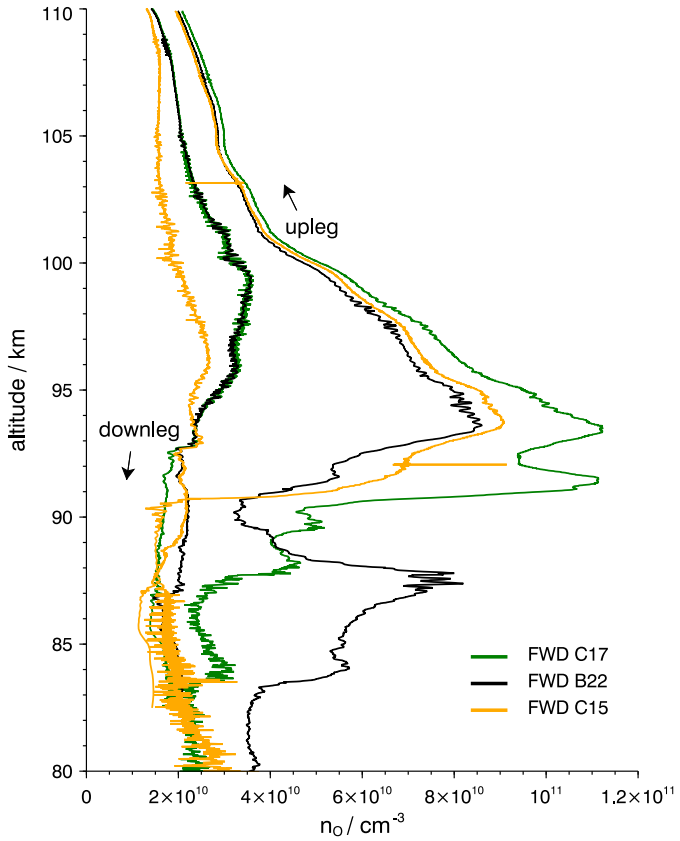

Figure 11. Measurement results for atomic oxygen number density vs. altitude for sensors on fore deck during up- and downleg without aerodynamic correction.

AMTD
8, 3245–3282, 2015

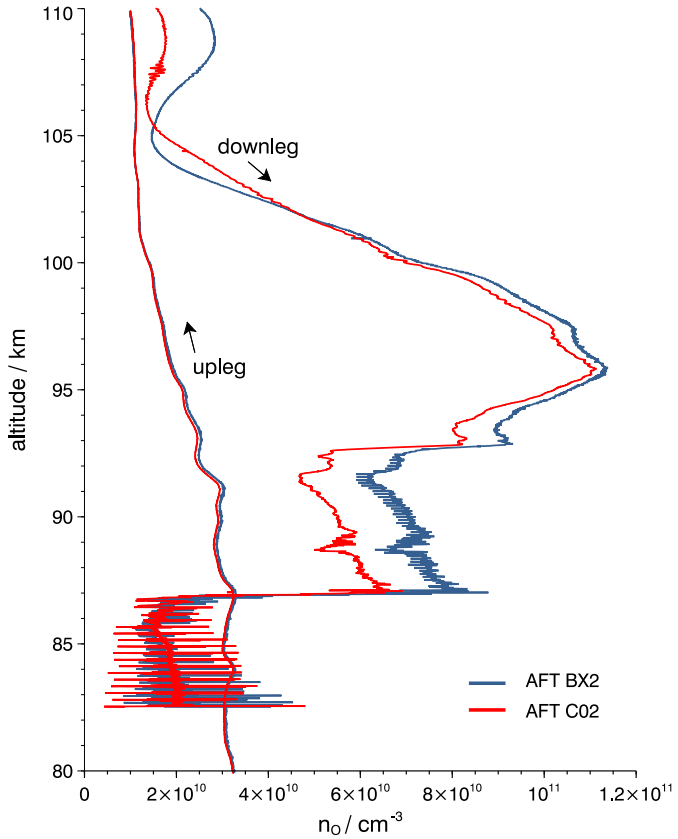

Figure 12. Measurement results for atomic oxygen number density vs. altitude for sensors on aft deck during up- and downleg without aerodynamic correction.

AMTD
8, 3245–3282, 2015

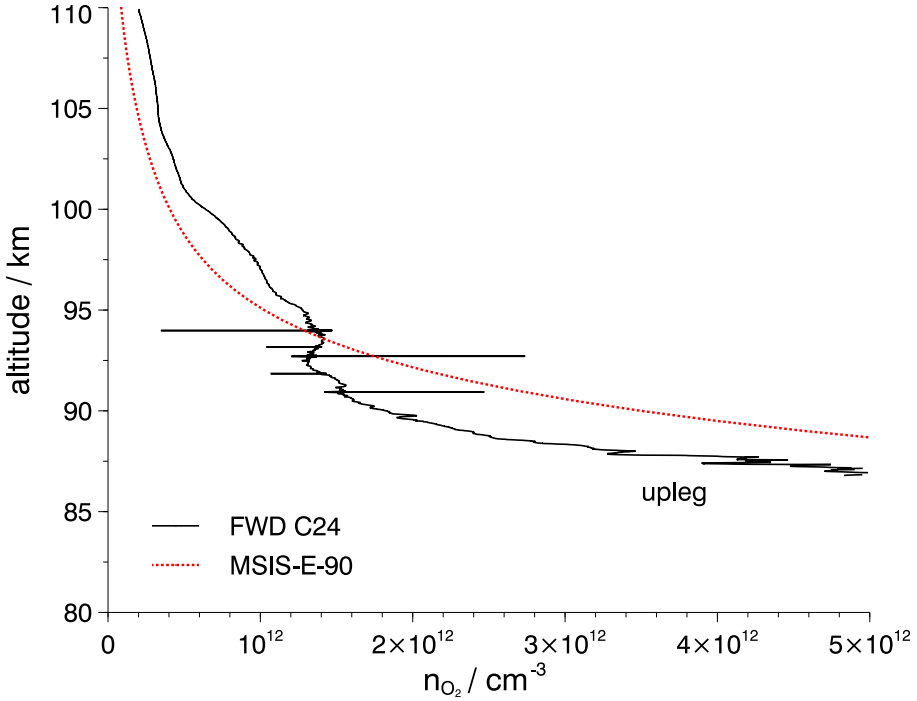

Figure 13. Profile for the O_2 (+O) number density from fore sensor C24 after aerodynamic correction compared to MSIS-E-90.

AMTD
8, 3245–3282, 2015

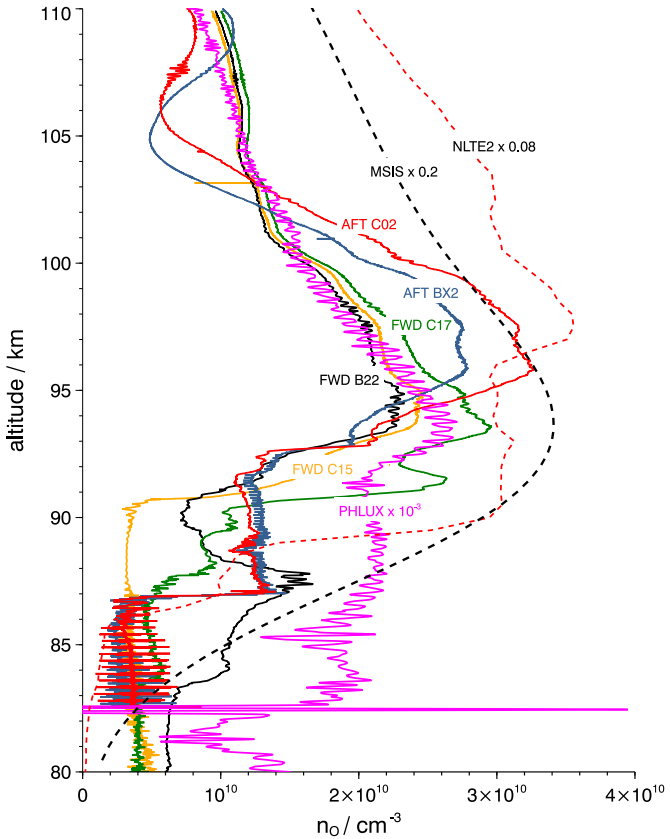

Figure 14. Profiles of O number density for FIPEX sensors on fore and aft deck after aerodynamic correction. Downleg profile for aft sensors, upleg part for the fore sensors. The PHLUX profile is scaled by a factor of 1×10^{-3} and is shifted by +16 km upwards. Comparison to MSIS model and NLTE-2 measurements.

AMTD
8, 3245–3282, 2015

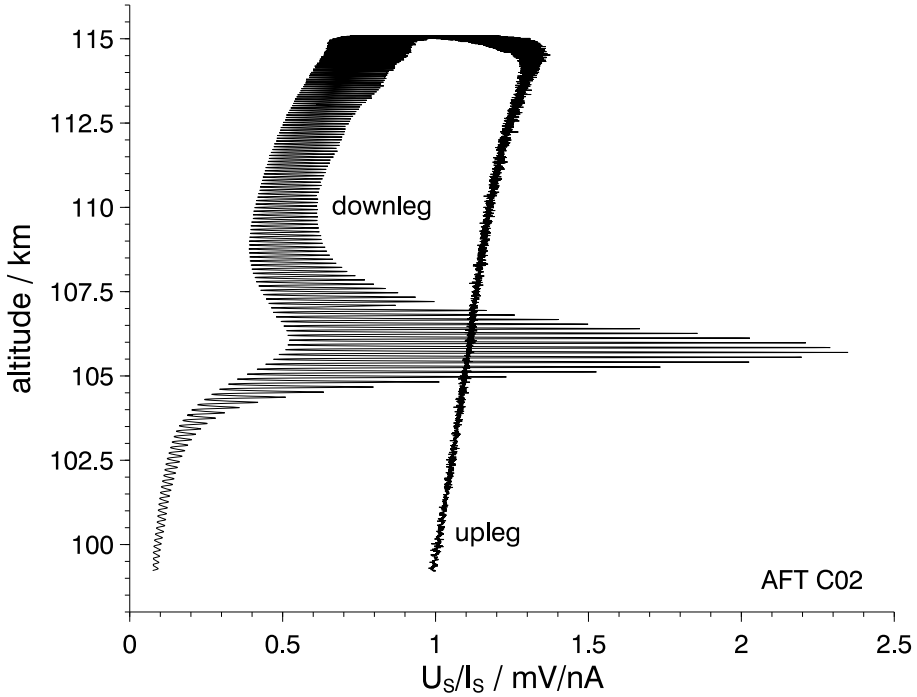

Figure 15. Ratio of voltage to current on an aft sensor during downleg. Raw values including 2.9 Hz modulation due to rocket spin.

AMTD
8, 3245–3282, 2015

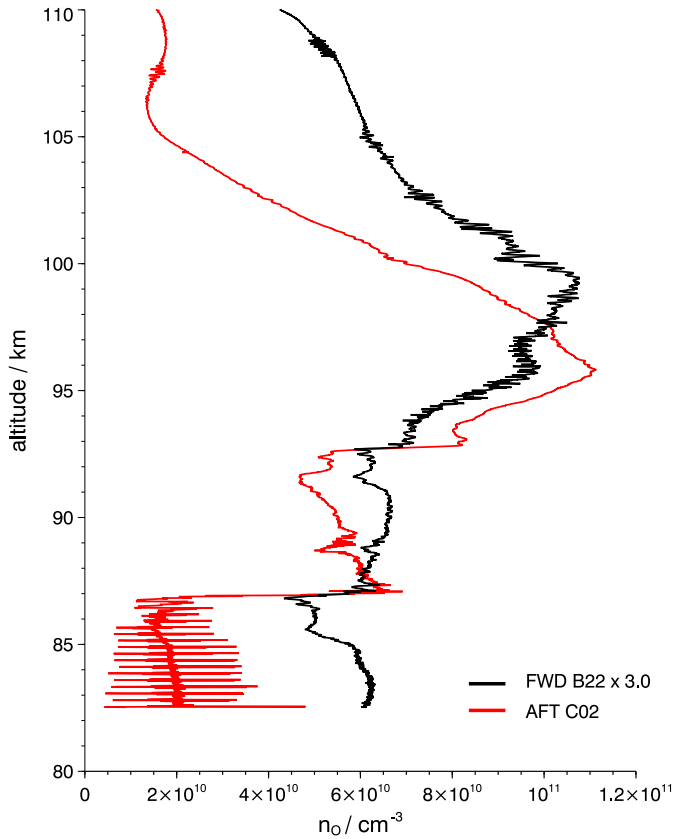

Figure 16. Comparison of density profiles from sensors on fore and aft deck during downleg without aerodynamic correction.

AMTD
8, 3245–3282, 2015